Optimized detection of somatic allelic imbalances specific for homologous recombination deficiency improves the prediction of clinical outcomes in ovarian cancer

Fernando Perez-Villatoro[1,2], Jaana Oikkonen[1], Julia Casado[1,2], Anastasiya Chernenko[1,2], Doga C. Gulhan[3], Manuela Tumiati[1], Yilin Li[1], Kari Lavikka[1], Sakari Hietanen[4], Johanna Hynninen[4], Ulla-Maija Haltia[5], Jaakko S. Tyrmi[6,7], Hannele Laivuori[6], Panagiotis Konstantinopoulos[9], Sampsa Hautaniemi[1], Liisa Kauppi[1,8], Anniina Färkkilä[1,2,5,9]

[1] Research Program for Systems Oncology, University of Helsinki, Helsinki, Finland
[2] iCAN digital precision cancer medicine flagship
[3] Department of Biomedical Informatics and Ludwig Center at Harvard, Harvard Medical School, Boston, MA, USA
[4] Department of Obstetrics and Gynecology, University of Turku and Turku University Hospital, Turku,Finland
[5] Department of Obstetrics and Gynecology, Helsinki University Hospital, Helsinki, Finland
[6] Faculty of Medicine and Health Technology, Center for Child, Adolescent, and Maternal Health, Tampere University Tampere, Finland
[7] Computational Medicine, Faculty of Medicine, University of Oulu, Oulu, Finland
[8] Department of Biochemistry and Developmental Biology, University of Helsinki, Helsinki, Finland
[9] Dana-Farber Cancer Institute, Harvard Medical School, Boston, USA

Correspondence:
Anniina Färkkilä, MD PhD, Docent in Translational Gynecologic Oncology
Principal Investigator, Academy of Finland Clinical Research Fellow
Specialist in Obstetrics and Gynecology

Research Program for Systems Oncology &
Department of Obstetrics and Gynecology
University of Helsinki and Helsinki University Hospital
00014 University of Helsinki
anniina.farkkila@helsinki.fi
+358505967786

ABSTRACT

Specific patterns of genomic allelic imbalances (AIs) have been associated with Homologous recombination DNA-repair deficiency (HRD). We performed a systematic pan-cancer characterization of AIs across tumor types, revealing unique patterns in ovarian cancer. Using machine learning on a multi-omics dataset, we generated an optimized algorithm to detect HRD in ovarian cancer (ovaHRDscar). ovaHRDscar improved the prediction of clinical outcomes in three independent validation cohorts (PCAWG, HERCULES, TERVA). Characterization of 98 spatiotemporally distinct tumor samples indicated ovary/adnex as the preferred site to assess HRD. In conclusion, ovaHRDscar improves the detection of HRD in ovarian cancer with the premise to improve patient selection for HR-targeted therapies.

INTRODUCTION

Ovarian cancer is one of the most lethal gynecological malignancies[1], and high-grade serous ovarian, peritoneal or fallopian tube cancer (HGSC) is the most common subtype causing 70-80% of all ovarian cancer-related deaths[2]. The majority of the HGSCs are diagnosed at an advanced stage, and the cornerstone of the treatment is first line cytoreductive surgery combined with DNA damaging chemotherapy. However, nearly all patients will develop a progressive disease and the 5-year survival is only 40%.

Around half of HGSC tumors are considered to harbor genomic alterations leading to defects in the homologous recombination (HR) DNA repair pathway[3]. HR-deficient (HRD) tumors are markedly sensitive to DNA damaging therapies such as platinum and Poly-ADP Ribose Polymerase (PARP) inhibitors[4]. Recently, large clinical trials have reported significant benefits from PARP inhibitors especially in patients with HRD tumors[5,6]. The HRD test used in the clinical trials is test based on allelic imbalances (AIs); 1) Large scale transitions (LSTs), which are two AIs of at least 10Mbs separated by no more of 3Mbs[7]; 2) Loss of heterozygosity (LOH) regions bigger than 15Mbs[8]; 3) Telomeric allelic imbalances (TAIs), which are AIs that extend to the telomeres[9]. However, the defining criteria for these AIs were originally designed using mostly breast cancer samples, therefore the details of the genomic instability occurring in HRD ovarian cancers have not been clearly defined. Herein, we show that ovarian cancers harbor distinct patterns of AIs as compared to other cancer types including triple negative breast cancer (TNBC). Using an iterative machine learning approach and The Cancer Genome Atlas (OVA-TCGA) multi-omics dataset, we present an optimized algorithm (ovaHRDscar) for HRD-specific AIs in ovarian cancer. We show that ovaHRDscar improves the detection of HRD and prediction of therapy responses and clinical outcomes in three independent clinical datasets as compared to previous algorithms. OvaHRDScar thus shows promise as a fully optimized algorithm that can be used to improve patient selection for PARP inhibitor therapies in HGSC.

RESULTS

Systematic PanCancer characterization shows unique features of allelic imbalances in ovarian cancer

To characterize the features of AIs across different cancer types, we analyzed AIs from SNP-array data in eighteen most represented cancer types available in the TCGA (**Fig. 1a**). We calculated the number of allelic imbalances and their median size per each sample. Interestingly, ovarian cancers had the highest number of AIs per sample (**Fig. 1b**), but with the lowest median size (**Fig. 1c**). Concordantly, ovarian cancers showed the highest levels of LOH events per sample (**Supplementary Fig. 1a**) although with one of the lowest median sizes (**Supplementary Fig. 1b).** We next performed hierarchical clustering using the median length and number of AIs per sample, and the skewness of the size distribution of the AIs per cancer type. The cancer types were clustered in two main clusters, one of those conformed by six cancer types (BLCA, STAD, LUSC, BRCA, LUAD, OV) with higher amounts of AIs but with a lower median length (upper cluster: **Fig. 1d**) and the second cluster conformed by the remaining twelve types of cancers (lower cluster: **Fig. 1d**). The same main clusters were generated when using only LOH events (**Supplementary Fig. 1c**).

Then, we compared specifically differences in AIs between ovarian cancer and TNBC, as both cancers were used to define the HRD test used in clinical assays[10] and are enriched in *BRCA* gene mutations[11]. We observed that ovarian cancer samples had a higher number of AIs as compared to TNBC (U test, p = 0.01, **Fig. 1e**). The difference in abundance of AIs between ovarian cancer and TNBC was evident specifically in *BRCA*wt tumors (U test, p = 1.1e-04, **Fig. 1g**), but not in *BRCA*mut tumors (**Fig. 1f**). Interestingly, ovarian cancers had lower levels of LOH events than TNBCs (U test, p = 0.01, **Supplementary Fig. 1d**), also among the *BRCA*mut samples (U test, p = 0.044, **Supplementary Fig. 1e**) but not in the *BRCA*wt samples (**Supplementary Fig. 1f**). We then compared the numbers of AIs of

different sizes between ovarian cancer and TNBC. When compared in all samples, ovarian cancers showed higher levels of AIs of different sizes while TNBC had higher level of LOH events (**Fig. 1h**). Interestingly, LOH events longer than 30Mb were in higher proportion in TNBC in *BRCA*wt samples and *BRCA*mut samples. These results thus highlight the different characteristics of AI events in ovarian cancer, especially in the *BRCA*wt tumors, as compared to other cancer types.

Machine-learning optimized ovaHRDscar improves the detection of HRD in ovarian cancer

The specific AIs that are quantified in the HRD test (HRD-AIs) were defined using mostly breast cancer samples or in a mixture with ovarian cancer samples[10]. To optimize the size selection criteria (cutoffs) of the HRD-AIs in ovarian cancer, we utilized ovarian cancer samples from the TCGA (OVA-TCGA) and its associated genomic and methylomics data. Importantly, in contrast to previous studies that focused on distinguishing specific AIs associated with *BRCA1/2* mutation status, we aimed to identify AIs overrepresented in samples carrying associated HRD alterations (mutations, gene deletions, promoter hypermethylation) compared to the HR proficient (HRP) samples (**Fig. 2a**). Via a systematic approach utilizing prior knowledge and deep multi-omics data, we identified 93 HRD samples harboring a somatic or germline mutation, gene deletion or promoter hypermethylation in the *BRCA1/2* or *RAD51* paralog genes (**Fig. 2a**). In contrast, we identified 34 HRP samples that do not harbor any of the alterations used to select HRD samples, nor deletion in any other HR gene. A detailed description of the genomic alterations in the samples is reported in **Supplementary Table 1**. Overall, the HRD samples had a higher amount of all AIs than the HRP samples quantified using SNP array data (**Supplementary Fig. 2a**). Importantly, the HRD samples had a notably higher proportion of AIs with specific sizes that span from 1Mbs to 30Mbs (**Supplementary Figs. 2b, c**), while the HRP samples contained a higher proportion of AIs and LOH events smaller than 1Mbs.

We next applied a decision-tree[12] machine learning classifier in an iterative approach to identify the specific sizes of LOH, LST and TAI events overrepresented in the HRD samples (**Fig. 2b**). This approach quantified the AIs of a given size, then evaluates independently 1) the difference in abundance of the selected AIs between the HRD versus the HRP samples and 2) the classification accuracy of HRD from the HRP samples by machine learning decision trees that took abundance of AIs as the splitting criteria. Optimization of LOH, LST and TAI events identified distinct AIs in ovarian cancer as compared to the HRD score used previously in clinical trials (hereafter called Telli2016). Importantly, the iterative approach increased the accuracy of classification of the HRD/HRP samples from 84.9% with the previous cutoffs to 89.4% with the optimized cutoffs for LOH events (**Fig. 2c**). For LSTs, the accuracy increased from 87.0% to 90.6% when using the optimized cutoffs (**Supplementary Fig. 2d**). We also assessed the classification accuracy of LST conformed by three consecutive AIs, however this produced a lower accuracy (**Supplementary Fig. 2e**). Similarly, for TAI events, the accuracy increased from 72.2% to 80.6% (**Supplementary Fig. 2f**). As the largest improvement in accuracy of TAI occurred after including TAIs larger than 1MBs, and inclusion of bigger sizes did not increase considerably the accuracy, we decided to ignore TAIs smaller than 1Mb rather than selecting TAIs with a specific size.

Via systematic optimization, we observed the following AIs to be characteristic of HRD in ovarian cancer: 1) LOH > 15Mb and <50Mb, 2) for LSTs AI > 12Mb with a space between them <1Mb and 3) TAI >1Mb. The sum of these events is hereafter called the ovaHRDscar levels. Then, we used the distribution of ovaHRDscar levels to determine the optimal cutoff value to separate HRD and HRP samples. The value that best separated the two distributions was 54 (**Fig. 2d**), meaning that values higher than 54 correspond to HRD, with a higher accuracy for HR status classification (BA=0.89) as compared to the Telli2016 cutoff of 42 (BA=0.79).

ovaHRDscar algorithm shows concordance in WGS data and correlates with mutational signature 3

In order to illustrate the relationships of ovaHRDscar with other known signatures associated with HRD, we annotated OVA-TCGA samples according to mutations, gene deletions and promoter hypermethylation patterns previously reported associated with HRD[3] (**Fig. 2e**). On average, samples with somatic mutations in *BRCA1*, *BRCA2*, *PTEN*, or somatic mutations or gene deletions in any gene belonging to the Fanconi Anemia (FA), or the HR pathways showed high ovaHRDscar levels. Likewise, samples that contained hypermethylation in the promoter regions of the genes *BRCA1* or *RAD51C*, or germline mutations in *BRCA1* or *BRCA2* had on average high ovaHRDscar levels. As predicted, samples harboring an amplification in *CCNE1* (**Supplementary Fig. 2g**) had significantly lower levels of ovaHRDscar. Remarkably, samples with *EMSY* amplification and *CDK12* somatic mutation also presented with low levels. Thus, in addition to the *BRCA1/2* or *RAD51* paralogs, all the groups of samples with any disruption in genes related to HRD, except those positive for *EMSY* amplification and *CDK12* somatic mutation, contained on average significantly higher levels of ovaHRDscar as compared to samples with *CCNE1* amplification (**Supplementary Fig. 2g**).

Next, we quantified the ovaHRDscar levels on whole genome sequencing (WGS) data of HGSC samples from the Pan-Cancer Analysis of Whole Genomes project (PCAWG)[13]. First, we evaluated the level of agreement of the ovaHRDscar levels between WGS and SNP-array data. For this we selected 41 OVA-TCGA samples that were also included in the PCAWG project. The ovaHRDscar levels were highly concordant between WGS and SNP-arrays (Lin's concordance correlation coefficient, ccc = 0.915; **Supplementary Fig. 2h**), this is consistent with a previous report in breast cancer samples that quantified AIs in the two platforms[14]. Next, we tested the correlation of ovaHRDscar with the single base substitution signature 3 (SBS3), which has been associated with HRD in human cancers samples[15]. We found that the ovaHRDscar levels detected in WGS positively correlated with the proportion

of SBS3 in WGS (Pearson, r'=0.37, p= 8.4e-05; **Fig. 2f**). In addition, we observed a significant correlation of ovaHRDscar from SNP arrays with SBS3 inferred from whole exome sequencing (WES) data using SigMA, a likelihood-based approach to identify samples enriched in SBS3[16] in OVA-TCGA (Pearson r'=0.5, p<2.2e-16; **Supplementary Fig. 2i**). The SBS3 proportions also correlated with the number of HRD-AIs using the Telli2016 algorithm in PCAWG (**Supplementary Fig. 2j**) and in OVA-TCGA (**Supplementary Fig. 2k**). The ovaHRDscar algorithm detected a total 149 samples as HRD (55%) and the SigMA tool classified 151 samples (56%) as SBS3+; in comparison, the Telli2016 algorithm identified 220 samples (81%) (**Fig. 2g**). Importantly, ovaHRDscar showed an improved agreement with SigMA (agreement 77% and cohen's kappa = 0.53) as compared to the Telli2016 algorithm (agreement 69.3% and cohen's kappa = 0.34; **Fig. 2g**).

ovaHRDscar improves the prediction of PFS and OS compared to previous algorithms

Next, we measured the association of HR-status classification by ovaHRDscar with progression free survival (PFS, see methods) in HGSC patients treated with platinum-based chemotherapy from the TCGA and from an independent validation dataset (HERCULES). We compared the performance of ovaHRDscar versus *BRCA1/2* deficiency status, the Telli2016 algorithm, and to a HRD/HRP cutoff value of 63 HRD-AIs as proposed by Tacaya et al[17]. As *BRCA1/2* mutations can affect patient outcomes, we assessed the performances of ovaHRDscar in the TCGA also after excluding the samples used in the training set, even though clinical outcomes were not utilized for the optimization. *BRCA1/2* mutation or deletion status (*BRCA*mut/del) was not significantly associated with PFS (log-rank p=0.72; **Fig. 3a**). For OVA-TCGA (**Fig. 3a to 2c**), we found that ovaHRDscar positivity was associated with prolonged PFS (log-rank p=6.2e-05; **Fig. 3c**) with smaller 95% confidence intervals and a lower p-value as compared to the Telli2016 algorithm (log-rank p=0.0024; **Fig. 3b**); the median PFS was 19.3 months for the ovaHRDscar positive patients and 17.8 months for the Telli2016 positive patients. Consistently, also in the HERCULES cohort, ovaHRDscar positive patients had a longer PFS (log-rank p=0.001; **Supplementary Fig.**

3c), while the Telli2016 algorithm was did not reach statistical significance in predicting PFS in the (log-rank p=0.07; **Supplementary Fig. 3b**).

We next used Cox proportional hazard models to assess the performance of the HRD classification status algorithms for predicting PFS outcomes. We adjusted for the presence of residual tumor after the primary debulking surgery, as that has been shown to be a strong independent prognostic factor for PFS[18]. We found that ovaHRDcar positivity was associated most significantly with a prolonged PFS in OVA-TCGA when adjusting for residual tumor (Wald test p=9.2e−08, **Fig. 3d**) outperforming the Telli2016 algorithm (Wald test p=2.9e−07) and the Tacaya algorithm (Wald test p=5.2e−06), also after excluding the samples used in the optimization (middle panel, **Fig. 3d**) and when not adjusting for the residual tumor (**Supplementary Fig. 3d**). In contrast to the previous algorithms, ovaHRDscar positivity was associated with longer PFS also in the independent HERCULES cohort (HR 0.359, Wald test p=0.0061).The results were similar in the most challenging patient population after excluding the *BRCA*mut/del samples from the cohorts (Lower panel, **Fig. 3d**). We inspected the performance of the HRD-classification algorithms in a second independent prospective cohort (TERVA) with tumor-only SNP array profiling performed with a panel of normals (see methods). Importantly, ovaHRDscar positivity most significantly predicted longer PFS using log-rank test and cox proportional hazard model (**Supplementary Fig. 3e to 3g**). For most of the comparisons these results were consistent in the non-adjusted Cox regression models (**Supplementary Fig. 3e**).

Subsequently, we next explored the association of ovaHRDscar with overall survival (OS) in HGSC patients in the OVA-TCGA cohort, and in an independent AU-OVA cohort in PCAWG. The clinical data in the prospective cohorts (HERCULES, TERVA) were not mature enough for OS evaluation. We found that both in the OVA-TCGA and PCAWG datasets, ovaHRDscar was superior to BRCA1/2 deficiency status, or to Tell2016 or Tacaya2020 algorithms (**Fig. 3g, Supplementary Fig. 3j**). In Cox regression analysis for OS using the

patient age at diagnosis as a covariable, ovaHRDscar had improved significance for predicting OS (**Fig. 3h**). Of note, the hazard-ratio values were lower in OVA-TCGA using the Telli2016 algorithm however the corresponding HR was not significant in the PCAWG cohort. Consistent with the PFS analysis, the ovaHRDscar hazard-ratios and significance were superior to the Tacaya2020 algorithm in all comparisons. These results were concordant also using a non-adjusted Cox regression analysis (**Supplementary Fig. 3k**). Additionally, we compared the performance of ovaHRDscar to the CHROD algorithm that uses structural variations and a random forest implementation to classify the HR status[19]. We found that ovaHRDscar showed an improved prediction of OS as compared to the CHORD algorithm using log-rank test (**Supplementary Fig. 3l, m**) and using cox proportional hazard models (**Supplementary Fig. 3n**) in the PCAWG cohort.

Low intra-patient variation of ovaHRDscar in spatiotemporal tumor profiling

We next explored whether the anatomical site or timing of sample retrieval causes a potential bias in the HR status classification in ovarian cancer. For this, we explored the concordance of ovaHRDscar levels in the HERCULES prospective cohort, which includes 89 tumor samples of different anatomical sites and different treatment phases (treatment naive, after neoadjuvant chemotherapy, or at relapse) from 33 HGSC patients (**Fig. 4a**). Consistent with the TCGA dataset, the ovaHRDscar levels corresponded with the known genomic predictors of HR status (**Fig. 4b**). Importantly, we found that the levels were similar in paired, anatomically matched samples obtained before and after neoadjuvant chemotherapy, and also in primary (treatment naive) as compared to relapsed tumors (**Fig. 4c**). Further, the intra-patient levels variability was not explained by the differences in tumor purity (minimum 30%, see methods) (**Supplementary Fig. 4b** and **Supplementary Fig. 4c**). We observed some intra-patient variation between the anatomical sites (**Fig. 4a**), however it was lower than the inter-patient variation (**U test p=1.95e-38; Supplementary Fig. 4a**). To determine the optimal anatomical sampling site, we next assessed the HR-status per patient in treatment-naive primary samples and compared ovaHRDscar calculated from specific

anatomical sites (or average if many samples per site) including 1) all samples (All) 2) ovarian (OVA) 3) ovarian or adnexal (OVA/ADN) 4) omentum, and OVA/ADN if omentum sample not available (OME-OVA/ADN) 5) OVA/ADN, and then omentum if OVA/ADN not available (OVA/ADN-OME). Overall, the level of agreement for the HR-status classification between the prioritization of anatomical sites ranged from 94% and 97% respectively (**Supplementary Fig. 4d**). Importantly, ovaHRDscar status calculated primarily from ovarian or adnexal tumor was the strongest predictor of PFS improvement (**Fig. 4d**, **Supplementary Fig. 4e**). Consistently, prioritizing ovarian tumors (OVA) classified all tumors harboring *CCNE1* amplification as HRP (**Supplementary Fig. 4d**).

DISCUSSION

HRD tumors exhibit a distinct clinical phenotype with superior responses to platinum-based chemotherapies and sensitivity to PARP inhibitors. Herein, we established ovaHRDscar, a systematically optimized biomarker for HRD to improve patient selection and clinical outcomes in ovarian cancer.

Several genomic approaches have been utilized to detect HRD, including 1) identification of single genetic mutations leading to predicted HRD[21], 2) profiles of DNA repair deficiency gene expression[22,23], 3) specific mutational patterns accumulated due to HRD[8,9,24] or 4) structural genomic imbalances[7,25]. These genomic features have been implemented either alone, or in combinations in the search for optimal HRD detection which has profound therapeutic implications[26]. It is now becoming accepted that benefit from HR-directed therapeutic such as PARP inhibitors extend beyond the identification of HRD via individual genetic mutations[27]. This is due to the facts that genes such as *BRCA1/2* and *RAD51* paralogs, can be altered beyond mutations e.g. via hypermethylation or gene deletions[3,28], and not all genomic events leading to HRD have yet been defined[29]. Allelic imbalances are indicative of the genetic consequences of HRD and, although not dynamically reflective of

tumors functional HRD status, have shown promise as a biomarker predictive for the magnitude of benefit from PARP inhibitors, especially in the front-line setting[30,31]. The HRD test used in the ovarian cancer clinical trials was, however, optimized using breast cancer samples or a mixture of breast cancer and ovarian cancer samples using *BRCA1/2* mutation as the sole denominator of HRD, and *BRCA*wt status as HRP[8,9,10]. Importantly, also European Society of Medical Oncology indicated an urgent need to optimize the HRD test in ovarian cancer to improve the identification of especially the HRP tumors[23]. Via a pan-cancer characterization of AIs, we observed marked differences in the AI patterns of ovarian cancer as compared to other cancer types including TNBC, especially among the *BRCA*wt tumors. This prompted us to systematically identify the genomic footprints of HRD-AIs in ovarian cancer using carefully annotated multi-omics data from the TCGA and an iterative machine learning and statistical approach.

ovaHRDscar levels were concordant with tumor genetic mutations and copy number events predictive of HRD status both in the TCGA dataset, and in an external validation cohort (HERCULES). We found significantly lower levels of ovaHRDscar in tumors with *CCNE1* amplification, proposed as mutually exclusive with HRD and associated with poor clinical outcomes[32]. In line with a previous report[17], tumors with *CDK12* mutation showed overall low levels of ovaHRDscar. Further, ovaHRDscar showed a higher concordance with mutational signature 3 as compared to the Telli2016 algorithm. Importantly, ovaHRDscar can be applied to detect HRD in HGSC samples using WGS or SNP-arrays, making it an attractive biomarker for the clinical setting.

A dichotomous thresholding of a predictive HRD biomarker is needed for therapeutic decision making. In Telli2016, the cutoff for the total number of events was derived from a mixture of breast and ovarian cancer samples[10]. More recently, Tacaya et al set out to improve the HRD test by adjusting the cutoff value in ovarian cancer[17], however only *BRCA*mut status was used for separating the HRD from HRP samples and the same

genomic features of HRD-AIs were used as in Telli et al. In ovaHRDscar, after optimization of both the genomic footprints of HRD-AIs, and the cutoff, we identified more samples as being HRP, and reliably separated HRD from HRP with improved accuracy as compared to the previous algorithms. In survival analyses, our fully optimized ovaHRDscar outperformed the two previous algorithms, indicating that both the identification of the genomic footprints of HRD-AIs, and the selection of the optimal cutoff are needed to improve HRD detection in ovarian cancer.

HRD tumors are known to have superior responses to platinum-based chemotherapy and prolonged overall survival[33]. Consistently, ovaHRDscar improved the prediction of PFS and OS for platinum-based chemotherapy in the OVA-TCGA, also after excluding the patients used in the training set, even though clinical outcomes were not used in the optimization. ovaHRDscar significantly predicted PFS and OS also among only the *BRCA*wt tumors. Importantly, ovaHRDscar improved the prediction of clinical outcomes in two independent patient cohorts, and in multivariable models after adjusting for clinical covariables, indicating that ovaHRDscar reliably captures the phenotypic clinical behavior of HRD ovarian cancers. ovaHRDscar levels correlated with genomic features and responses to platinum-based chemotherapy, however none of the clinical cohorts included patients treated with PARP inhibitors, and thus the potential predictive biomarker role of ovaHRDscar would require prospective validation in larger patient series.

Finally, as HGSC is characterized by marked intratumor heterogeneity, we tested whether the anatomical site of tumor sampling or the exposure to chemotherapy affect HRD assessment. Our analysis of 98 samples collected from different anatomical sites and treatment phases indicated that ovaHRDscar levels remain similar in spatiotemporally distinct samples from each patient, including anatomically site-matched samples collected before and after neoadjuvant chemotherapy. ovaHRDscar can thus be reliably assessed during routine clinical practice also after neoadjuvant chemotherapy, given that the tumor

purity remains higher than 30%. Interestingly, the ovaHRDscar levels were also similar between treatment naïve and relapsed tumors, reflecting the nature of HRD-AIs as historical consequences rather than dynamic readouts of functional HRD. Overall, the interpatient variation was higher than the intrapatient variation, however in four out of 21 (19%) of patients the HRD category was dependent on the sampling site/time. The survival and genetic analyses indicated that ovarian or adnexal sites followed by omentum could be the preferred sites for HRD testing, warranting future validation in larger cohorts.

In conclusion, ovaHRDscar shows promise as a fully optimized, robust, clinically feasible assay for both outcome prediction and selection of patients to HR-directed therapies. With the fully documented, publicly available algorithms and optimization pipeline our method can be implemented clinically and applied to other tumor types for optimized patient selection and to improve outcomes in cancer.

MATERIAL AND METHODS

Data set collection and classification

For PanCan samples, Allele-specific copy number segments were obtained from the Genomics Data Commons (GDC) portal (https://portal.gdc.cancer.gov/). TNBC were defined as those breast cancers marked as negative by *er_status_by_ihc*, *pr_status_by_ihc* and *her2_status_by_ihc* in the clinical file "*nationwidechildrens.org_clinical_patient_brca.txt*" available in the GDC. For TNBC, samples were considered with *BRCA*mut if reported in Knijnenburg et al 2018[34] with gene deletion, gene mutation or gene silencing in *BRCA*1 or *BRCA*2 genes; while *BRCA*wt those reported with information of no alterations.

For OVA-TCGA analysis: Allele-specific copy number segments, DNA methylation, gene-level CNV profiles and clinical information data was obtained from the GDC data portal. Genes were considered with a "strong signal of deletion" if those were reported (labeled by -2) by Taylor et al 2018[35] and with signal of deletion those reported in the GDC portal. Gene

promoter hypermethylation was considered when the probes upto 1500bp downstream the transcription start site had an average beta value ≥0.75. The catalog of mc3 somatic mutations was obtained from the PanCanAtlas-GDC data portal (https://gdc.cancer.gov/about-data/publications/pancanatlas). Somatic mutations were classified according to the recommendations of the American College of Medical Genetics and Genomics[36] using the web-tool VarSome[37] only pathogenic somatic mutations were considered in the analysis. For germline mutations we selected those labeled as pathogenic and prioritized by Huang et al 2018[38]. Genes were considered part of the HR pathway, or other associated pathways according to the Kyoto Encyclopedia of Genes and Genomes database[39]. Complementary clinical information was obtained from the PanCanAtlas-GDC data portal. For PCAWG: Allele-specific copy number segments, mutational drivers and clinical information was obtained from the International Cancer Genome Consortium data portal (https://dcc.icgc.org/pcawg).

HRD-AI optimization

Firstly, we manually cataloged the OVA-TCGA samples as HRD and HRP according to the criteria in **Fig. 2a**. Then, for each of the HRD and HRP samples we identified HRD-AIs as reported by Marquard et al 2015[40] using an in-home built R package. Iteratively we assessed LOH events of different minimum sizes *i* and maximum sizes *L*, Large scale transitions (LST: two allelic imbalances of a size *S* separated by a genomic distance no longer than *M*) of different *S* and *M* values and telomeric allelic imbalances (TAI) of a minimum size *j*. For each of the combination of parameters *i* and *L, S* and *M, and j* it was computed 1) The mean difference in abundance of the corresponding HRD-AIs in HRD samples vs HRP samples using a one tailed Mann Whitney U test. 2) Classification of samples using decision trees by the R package 'rpart'; classification was performed according to the abundance of the selected HRD-AIs, samples above the decision tree's split-point value were considered as HRD and those bellow HRP (**Fig. 2b**). For each iteration (combination of parameters), the accuracy of the classifier was assessed using balanced accuracy (BA, which correspond to

the average value of the “true positive rate” and “true negative rate”), taking the manual categorization of HRD and HRP samples as ground true. Finally, the combination of values for *i* and *L, S* and *M*, and j, with the highest product of -log10(U test p-value) multiplied by the BA were selected for ovaHRDscar.

Survival analysis

Survival plots, log-rank test and cox regression models were performed with an R script using the package ‘survminer’ and ‘survival’. Data from patients treated by cisplatin or carboplatin was selected. For PCAWG, data from all patients was used (no treatment information available). Only data from primary samples (treatment naive) were used. *BRCA*mut/del status included pathogenic mutations, germline mutations and gene deletions with a “strong signal of deletion” as described above. Residual tumor after surgery was categorized as present or absent. For indicated cox regressions, the residual tumor status or patient age at diagnosis was used as a covariable. Progression free survival (PFS) and overall survival (OS) was defined as in Liu et al 2018[41]. The CHROD signature HR status classification for PCAWG samples was adopted from Nguyen et al 2020[19].

Prospective HERCULES and TERVA data analysis

The tumor samples were prospectively collected in the HERCULES (http://www.project-hercules.eu) and TERVA projects (https://www.healthcampusturku.fi/innovation-new/terva-project/). The Ethics Committee of the Hospital District of Southwest Finland, approved both studies ETMK Dnro: 145 /1801/2015. All patients gave their informed consent. For HERCULES, paired fresh tumor samples and blood normal samples were sequenced using Illumina-Hiseq WGS. Alignment to the human genome GRCh38 was done using the burrows wheeler aligner BWA-MEM[42]. Mutations were detected using GATK4-Mutect2 approach[43]. Mutect2 was used for detection of allele specific copy numbers. Calculation of tumor purity was estimated in two ways: 1) Based in somatic copy-number profiles using the software Ascat[44] 2) Based in *TP53* variant allele frequency (*TP53*-VAF), purity was estimated using

the formula: *2 / ((CN / TP53-VAF) - (CN - 2)),* where CN corresponds to the copy-number value in the corresponding somatic mutations in *TP53*; subsequently the higher purity value was selected. For the TERVA samples tumor-only profiling, the tumor samples were genotyped using the Infinium™ Global Screening Array-24 v2.0. B allele frequency and LogR ratios per sample probe was calculated using Illumina-GenomeStudio. Ascat software was used for the detection of allele specific copy numbers, *ascat.predictGermlineGenotypes* module was performed adjusting parameters according to a panel of 200 normal germline blood samples.

Statistics

The statistics analysis was performed in R. Difference in mean abundances was calculated using Mann Whitney U test. The distribution Skewness of AI sizes in different types of cancers was performed using the package DescTools. Agreement was calculated using the Cohen kappa test. Concordance was measured using Lin's concordance correlation coefficient. Level of correlations was assessed using Pearson correlations. P value less than 0.05 was considered statistically significant.

Code Availability

The code used to perform the AI optimization is available on Github: (https://github.com/farkkilab/findHRDsignatures), ovaHRDscar implementation is available as and R package on Github (https://github.com/farkkilab/ovaHRDscar).

Data availability

Data available upon request.

ACKNOWLEDGMENTS

Sigrid Jusélius Foundation (AF), Finnish cancer society (AF, JC), Academy of Finland (AF, grant numbers 314394 and 322178 to LK, grant number 314398 to SaHi), Paolo Foundation (AF), The Finnish Medical Foundation (AF), Finnish Cultural Foundation (AF), Instrumentarium Foundation (AF, JC), University of Helsinki (AF), the European Union's Horizon 2020 research and innovation program under grant agreement No 667403 for HERCULES (SHa, JH, SHi) and No 965193 for DECIDER (SHa, JH, SHi). FIMM genomics core facility. We would like to thank the FINNPEC for the statistical reference data.

COMPETING INTEREST

The authors declare no competing interests

Supplementary Information is available for this paper

REFERENCES

1 Reid, B. M., Permuth, J. B. & Sellers, T. A. Epidemiology of ovarian cancer: a review. *Cancer Biol Med* **14**, 9-32, doi:10.20892/j.issn.2095-3941.2016.0084 (2017).

2 Torre, L. A. *et al.* Ovarian cancer statistics, 2018. *CA Cancer J Clin* **68**, 284-296, doi:10.3322/caac.21456 (2018).

3 Konstantinopoulos, P. A., Ceccaldi, R., Shapiro, G. I. & D'Andrea, A. D. Homologous Recombination Deficiency: Exploiting the Fundamental Vulnerability of Ovarian Cancer. *Cancer Discov* **5**, 1137-1154, doi:10.1158/2159-8290.CD-15-0714 (2015).

4 Lord, C. J. & Ashworth, A. PARP inhibitors: Synthetic lethality in the clinic. *Science* **355**, 1152-1158, doi:10.1126/science.aam7344 (2017).

5 Ray-Coquard, I. *et al.* Olaparib plus Bevacizumab as First-Line Maintenance in Ovarian Cancer. *N Engl J Med* **381**, 2416-2428, doi:10.1056/NEJMoa1911361 (2019).

6 Gonzalez-Martin, A. *et al.* Niraparib in Patients with Newly Diagnosed Advanced Ovarian Cancer. *N Engl J Med* **381**, 2391-2402, doi:10.1056/NEJMoa1910962 (2019).

7 Popova, T. *et al.* Ploidy and large-scale genomic instability consistently identify basal-like breast carcinomas with BRCA1/2 inactivation. *Cancer Res* **72**, 5454-5462, doi:10.1158/0008-5472.CAN-12-1470 (2012).

8 Abkevich, V. *et al.* Patterns of genomic loss of heterozygosity predict homologous recombination repair defects in epithelial ovarian cancer. *Br J Cancer* **107**, 1776-1782, doi:10.1038/bjc.2012.451 (2012).

9 Birkbak, N. J. *et al.* Telomeric allelic imbalance indicates defective DNA repair and sensitivity to DNA-damaging agents. *Cancer Discov* **2**, 366-375, doi:10.1158/2159-8290.CD-11-0206 (2012).

10 Telli, M. L. *et al.* Homologous Recombination Deficiency (HRD) Score Predicts Response to Platinum-Containing Neoadjuvant Chemotherapy in Patients with Triple-Negative Breast Cancer. *Clin Cancer Res* **22**, 3764-3773, doi:10.1158/1078-0432.CCR-15-2477 (2016).

11 Stefansson, O. A. *et al.* Genomic profiling of breast tumours in relation to BRCA abnormalities and phenotypes. *Breast Cancer Res* **11**, R47, doi:10.1186/bcr2334 (2009).

12 Breiman, L. *Classification and regression trees*. (Wadsworth International Group, 1984).

13 Consortium, I. T. P.-C. A. o. W. G. Pan-cancer analysis of whole genomes. *Nature* **578**, 82-93, doi:10.1038/s41586-020-1969-6 (2020).

14 de Luca, X. M. *et al.* Using whole-genome sequencing data to derive the homologous recombination deficiency scores. *NPJ Breast Cancer* **6**, 33, doi:10.1038/s41523-020-0172-0 (2020).

15 Alexandrov, L. B. *et al.* The repertoire of mutational signatures in human cancer. *Nature* **578**, 94-101, doi:10.1038/s41586-020-1943-3 (2020).

16 Gulhan, D. C., Lee, J. J., Melloni, G. E. M., Cortes-Ciriano, I. & Park, P. J. Detecting the mutational signature of homologous recombination deficiency in clinical samples. *Nat Genet* **51**, 912-919, doi:10.1038/s41588-019-0390-2 (2019).

17 Takaya, H., Nakai, H., Takamatsu, S., Mandai, M. & Matsumura, N. Homologous recombination deficiency status-based classification of high-grade serous ovarian carcinoma. *Sci Rep* **10**, 2757, doi:10.1038/s41598-020-59671-3 (2020).

18 Polterauer, S. *et al.* Prognostic value of residual tumor size in patients with epithelial ovarian cancer FIGO stages IIA-IV: analysis of the OVCAD data. *Int J Gynecol Cancer* **22**, 380-385, doi:10.1097/IGC.0b013e31823de6ae (2012).

19 Nguyen, L., J, W. M. M., Van Hoeck, A. & Cuppen, E. Pan-cancer landscape of homologous recombination deficiency. *Nat Commun* **11**, 5584, doi:10.1038/s41467-020-19406-4 (2020).

20 Barretina-Ginesta, M. P. DNA damaging agents in ovarian cancer. *EJC Suppl* **15**, 67-72, doi:10.1016/j.ejcsup.2020.06.001 (2020).

21 Wagle, N. *et al.* High-throughput detection of actionable genomic alterations in clinical tumor samples by targeted, massively parallel sequencing. *Cancer Discov* **2**, 82-93, doi:10.1158/2159-8290.CD-11-0184 (2012).

22 Kang, J., D'Andrea, A. D. & Kozono, D. A DNA repair pathway-focused score for prediction of outcomes in ovarian cancer treated with platinum-based chemotherapy. *J Natl Cancer Inst* **104**, 670-681, doi:10.1093/jnci/djs177 (2012).

23 Konstantinopoulos, P. A. *et al.* Gene expression profile of BRCAness that correlates with responsiveness to chemotherapy and with outcome in patients with epithelial ovarian cancer. *J Clin Oncol* **28**, 3555-3561, doi:10.1200/JCO.2009.27.5719 (2010).

24 Wang, Y. K. *et al.* Genomic consequences of aberrant DNA repair mechanisms stratify ovarian cancer histotypes. *Nat Genet* **49**, 856-865, doi:10.1038/ng.3849 (2017).

25 Polak, P. *et al.* A mutational signature reveals alterations underlying deficient homologous recombination repair in breast cancer. *Nat Genet* **49**, 1476-1486, doi:10.1038/ng.3934 (2017).

26 Swisher, E. M. *et al.* Rucaparib in relapsed, platinum-sensitive high-grade ovarian carcinoma (ARIEL2 Part 1): an international, multicentre, open-label, phase 2 trial. *Lancet Oncol* **18**, 75-87, doi:10.1016/S1470-2045(16)30559-9 (2017).

27 Miller, R. E. *et al.* ESMO recommendations on predictive biomarker testing for homologous recombination deficiency and PARP inhibitor benefit in ovarian cancer. *Ann Oncol* **31**, 1606-1622, doi:10.1016/j.annonc.2020.08.2102 (2020).

28 Golmard, L. *et al.* Contribution of germline deleterious variants in the RAD51 paralogs to breast and ovarian cancers. *Eur J Hum Genet* **25**, 1345-1353, doi:10.1038/s41431-017-0021-2 (2017).

29 Radhakrishnan, S. K., Jette, N. & Lees-Miller, S. P. Non-homologous end joining: emerging themes and unanswered questions. *DNA Repair (Amst)* **17**, 2-8, doi:10.1016/j.dnarep.2014.01.009 (2014).

30 Ray-Coquard, I. *et al.* Olaparib plus Bevacizumab as First-Line Maintenance in Ovarian Cancer. *N Engl J Med* **381**, 2416-2428, doi:10.1056/NEJMoa1911361 (2019).

31 Gonzalez-Martin, A. *et al.* Niraparib in Patients with Newly Diagnosed Advanced Ovarian Cancer. *N Engl J Med* **381**, 2391-2402, doi:10.1056/NEJMoa1910962 (2019).

32 Etemadmoghadam, D. *et al.* Synthetic lethality between CCNE1 amplification and loss of BRCA1. *Proc Natl Acad Sci U S A* **110**, 19489-19494, doi:10.1073/pnas.1314302110 (2013).

33 Norquist, B. M. *et al.* Mutations in Homologous Recombination Genes and Outcomes in Ovarian Carcinoma Patients in GOG 218: An NRG Oncology/Gynecologic Oncology Group Study. *Clin Cancer Res* **24**, 777-783, doi:10.1158/1078-0432.CCR-17-1327 (2018).

34 Knijnenburg, T. A. *et al.* Genomic and Molecular Landscape of DNA Damage Repair Deficiency across The Cancer Genome Atlas. *Cell Rep* **23**, 239-254 e236, doi:10.1016/j.celrep.2018.03.076 (2018).

35 Taylor, A. M. *et al.* Genomic and Functional Approaches to Understanding Cancer Aneuploidy. *Cancer Cell* **33**, 676-689 e673, doi:10.1016/j.ccell.2018.03.007 (2018).

36 Richards, S. *et al.* Standards and guidelines for the interpretation of sequence variants: a joint consensus recommendation of the American College of Medical Genetics and Genomics and the Association for Molecular Pathology. *Genet Med* **17**, 405-424, doi:10.1038/gim.2015.30 (2015).

37 Kopanos, C. *et al.* VarSome: the human genomic variant search engine. *Bioinformatics* **35**, 1978-1980, doi:10.1093/bioinformatics/bty897 (2019).

38 Huang, K. L. *et al.* Pathogenic Germline Variants in 10,389 Adult Cancers. *Cell* **173**, 355-370 e314, doi:10.1016/j.cell.2018.03.039 (2018).

39 Kanehisa, M. & Goto, S. KEGG: kyoto encyclopedia of genes and genomes. *Nucleic Acids Res* **28**, 27-30, doi:10.1093/nar/28.1.27 (2000).

40 Marquard, A. M. *et al.* Pan-cancer analysis of genomic scar signatures associated with homologous recombination deficiency suggests novel indications for existing cancer drugs. *Biomark Res* **3**, 9, doi:10.1186/s40364-015-0033-4 (2015).

41 Liu, J. *et al.* An Integrated TCGA Pan-Cancer Clinical Data Resource to Drive High-Quality Survival Outcome Analytics. *Cell* **173**, 400-416 e411, doi:10.1016/j.cell.2018.02.052 (2018).

42 Li, H. & Durbin, R. Fast and accurate short read alignment with Burrows-Wheeler transform. *Bioinformatics* **25**, 1754-1760, doi:10.1093/bioinformatics/btp324 (2009).

43 Cibulskis, K. *et al.* Sensitive detection of somatic point mutations in impure and heterogeneous cancer samples. *Nat Biotechnol* **31**, 213-219, doi:10.1038/nbt.2514 (2013).

44 Van Loo, P. *et al.* Allele-specific copy number analysis of tumors. *Proc Natl Acad Sci U S A* **107**, 16910-16915, doi:10.1073/pnas.1009843107 (2010).

FIGURE LEGENDS

Figure 1. Pan-cancer characterization of AIs reveal unique patterns in ovarian cancer. **a** Types of cancer with more than 200 samples selected from TCGA, their corresponding number of samples are shown in the bars. **b** Number of AIs bigger than 3Mb and smaller than 50Mb per sample, ovarian cancer shows the highest abundance of AIs. **c** Median length of AIs (bigger than 3Mb and smaller than 50Mb) per sample, ovarian cancer shows the lowest median size per sample. **d** Hierarchical clustering for the types of cancer using as variables the median length, median number of AIs per sample and the skewness of the distribution of AIs sizes. **e** Ovarian cancer samples show a higher amount of AIs than TNBC (U test, p=0.01). **f** Comparison of *BRCA*mut samples (somatic deletion, promoter hypermethylation and gene deletions of *BRCA*1/2 genes), shows not significantly higher amounts (U test) of AIs in ovarian cancer than in TNBC. **g** Comparison of *BRCA*wt samples, shows higher amounts of AIs in ovarian cancer than in TNBC (U test, p=1.1e-04). **h** Difference in abundance for AIs of specific sizes between ovarian cancer and TNBC, dot sizes correspond to U test p values and dot colors to the fold change (ratio of ovarian-TNBC median abundance of AIs minus one), only dots for corresponding significantly differences are shown (U test, $p < 0.05$).

Figure 2. Optimization of size selection for AIs associated with HRD in ovarian cancer and relationship with HRD biomarkers. a Selection criteria for HRD, HRP and Undefined samples in OVA-TCGA. **b** A schematic of the approach used to optimize the size selection

criteria (cutoff) of HRD-AIs in ovarian cancer samples. Iteratively, AIs of different sizes were taken, in each iteration it was evaluated: 1) the difference of abundance (U test) of the selected AIs between HRD versus HRP samples, 2) the accuracy of a decision tree classifier for HR status taking as splitting criteria the abundance of the selected AIs; all results were stored and the best cutoffs were selected for the ovaHRDscar. **c** For LOH events, the size of dots represent the decision tree balanced accuracy (BA) when using the corresponding AIs sizes, colors correspond to the statistical (U test, p value) difference in abundance of AIs between HRD versus HRP samples; black box correspond to the selection criteria proposed by Telli2016, blue box correspond to the best BA value. **d** Density distribution of HRD-AIs according to Telli2016 and ovaHRDscar algorithms. The red dashed line represents the cutoff established to define HRD or HRP samples for Telli2016 (>= 42) and for ovaHRDscar (>= 54), the blue dashed line in the left panel represents the cutoff proposed in Tacaya et al. 2020 (>= 63). The balanced accuracy (BA) for classifying the HR status is shown for Telli2016 and ovaHRDscar. **e** Levels of ovaHRDscar in OVA-TCGA samples harboring different genetic or epigenetic alterations associated with HRD in ovarian cancer[3]. In the outer ring of the pie chart every line represents a sample; in the center of the pie chart the colors correspond to the average number of HRD-AIs per genetic or epigenetic alteration. Somatic mutations included gene deletions. **f** The proportion of single base substitution signature 3 (SBS3) is correlated (Pearson r'=0.37) with the number of ovaHRDscar in PCAWG samples. **g** The SBS3 status inferred by SigMA has a higher agreement with ovaHRDscar (agreement=77%, cohen's kappa = 0.53) than with the Telli2016 algorithm (agreement=69.3%, cohen's kappa = 0.34), in the pie charts and table + and - correspond respectively to the number of HRD positive and HRD negative samples identified under each criteria. In the button is shown the number of samples selected under the corresponding criteria and the level of agreement.

Figure 3. HRD detected by ovaHRDscar is associated with higher PFS and OS in HGSC patients treated with platinum. a to c Kaplan-Meier plots of PFS in OVA-TCGA

patients stratified with different criteria, in **a** patients were stratified according to *BRCA*mut/del status with no significant difference in their PFS probability over time (log-rank, p=0.72); in **b** patients were stratified according to Telli2016 (log-rank, p=0.0024); in **c** patients were stratified using the ovaHRDscar algorithm, HRD patients had a improvement in PFS time over HRP (log-rank, p=6.2e-05). **d** Cox regression results for the association of PFS with several genomic HR status classification criteria (*BRCA*mut/del, Telli2016, Tacaya2020, ovaHRDscar) in two independent cohorts, for every regression it was used as covariable the residual tumor status (yes or no) after surgery. Three panels are shown: at left the OVA-TCGA cohort, at the middle OVA-TCGA cohort excluding the HRD and HRP samples used for the HRD-AIs optimization, at the right the HERCULES WGS prospective cohort. Inside each panel is shown for classification criteria: the number of patients (N) selected as positive or HRD and their corresponding proportion (Prop), the hazard-ratio (HR) for the cox regression and the p-value (Pval) of the regression. ovaHRDscars show higher significance (lower p values) in every cohort even after excluding patients with tumors harboring *BRCA*mut/del (bottom section). **e to g,** Kaplan-Meier plots of OS for OVA-TCGA patients selected using different criteria, ovaHRDscar show the higher significance (lower long-rank test p-values). **h** Cox regression results for the association of OS with several genomic HR status classification criteria (*BRCA*mut/del, Telli2016, Tacaya2020, ovaHRDscar) in two independent cohorts. Panel at the right corresponds to the AU-PCAWG samples, the left and center panels and their corresponding columns correspond to those described in Fig. 3d. ovaHRDscars show higher significance (lower p values) in every cohort even after excluding patients with tumors harboring *BRCA*mut/del (bottom section).

Figure 4. Low intra-patient anatomical variation of ovaHRDscar. a An overview of the samples and their corresponding ovaHRDscar levels per patient inside a prospective cohort analyzed by WGS (HERCULES). Per patient tumor samples were taken in three different treatment times and from different anatomical sites as described; in parentheses are displayed the corresponding number of samples. **b** Levels of ovaHRDscar in samples

harburing different genetic or epigenetic alterations associated with HRD, in the outer ring of the pie chart every bar represents a sample carrying the corresponding alteration; in the center of the pie chart the colors correspond to the average levels of ovaHRDscar per alteration. **c** ovaHRDscar values between paired samples for each patient (connected dots) does not vary significantly (paired U test) over treatment phase. **d** Cox regression results for the association of PFS with HR status classification by Telli2016 and ovaHRDscar, the HR status per patient was assessed using three anatomical sample prioritization approaches: 1) average HRD-AIs per all samples 2) omentum, and OVA/ADN if omentum sample not available (OME-OVA/ADN) 3) OVA/ADN, and then omentum if OVA/ADN not available (OVA/ADN-OME). Last prioritization approach has a higher association with PFS.

SUPPLEMENTARY FIGURE LEGENDS

Supplementary Figure 1. Pan-cancer characterization of LOH and unique patterns in ovarian cancer. a. Boxplot for the number of LOH bigger than 3Mb and smaller than 50Mb per sample, ovarian cancer shows the higher abundance of LOH. **b** Median length of LOH (bigger than 3Mb and smaller than 50Mb) per sample. **c** Hierarchical clustering of the types of cancer using as variables the median length, median number of LOH per sample and the skewness of the distribution of LOH sizes. **d** Ovarian cancer samples show a lower amount of LOH than TNBC (U test, p=0.005). **e** Comparison of *BRCA*mut samples (somatic deletion, promoter hypermethylation and gene deletions of *BRCA*1/2 genes), ovarian cancer shows higher amounts of LOH than TNBC (U test, p=0.044). **f** Comparison of *BRCA*wt samples, not significant abundance difference of LOH (U test, NS) between ovarian cancer and TNBC.

Supplementary Figure 2. Descriptive statistics of HRD and HRP ovarian samples, optimization of HRD selection. a Number of allelic imbalances in HRD and HRP samples in OVA-TCGA, in average HRD samples contain a higher number of allelic imbalances (U

test, p value=1.99e-05). **b** The average proportion of segments (AI or normal) equal or greater than the given size in HRD (red) and HRP (blue) samples, the blue and red lines correspond to smoothing using cubic splines. **c** Density distribution of LOH events in HRD (red) and HRP (blue) samples. **d** LSTs specific AIs size cutoffs (blue boxes) uperform the reported by Telli et al 2016 (black box); the size of dots represent the decision tree balanced accuracy (BA) when using the corresponding cutoff, colors correspond to the statistical (U test p value) difference in abundance of AIs between HRD versus HRP samples. **e** Statistical significance for identifying HRD samples using three tandem allelic imbalances LSTs of a given minimum size (x axis) and distance between them smaller than 1 to 4 Mb (y axis). Dot sizes and colors resemble those in Supplementary Figure 1e. **f** The selection of TAIs >1Mb differentiate HRD from HRP samples better than using all size TAIs, the upper panel shows statistical (U test, p values) difference in abundance of AIs between HRD versus HRP samples when selecting the corresponding TAIs, dot sizes and colors in the lower panel correspond to the description in panel d and e. **g** ovaHRDscar levels per genomic alteration in OVA-TCGA, U test p values are shown for the comparison of levels between the corresponding alterations versus CCNE1 amplification. **h** Bland-Altman plot that shows the concordance (Concordance correlation coefficient, *CCC* = 0.915) between the number of ovaHRDscars detected by SNP-arrays and WGS in the intersecting samples from OVA-TCGA and PCAWG. **i** Correlation (Pearson, r=0.5) between the SBS3 exposure in WES data from OVA-TCGA inferred using SigMA versus the number of ovaHRDscars in SNP arrays. **j** Correlation (Pearson, r=0.38) between the SBS3 proportion in WGS data from PCAWG versus the number of scars using the Telli2016 approach. **k** Correlation (Pearson, r=0.51) between the SBS3 exposure in WES data from OVA-TCGA inferred using SigMA versus the number of scars using the Telli2016 approach in SNP arrays.

Supplementary Figure 3. HRD detected by ovaHRDscar is associated with better PFS and OS in ovarian cancer patients after normalizing with relevant covariables. a to c Kaplan-Meier plots of PFS in HERCULES cohort, the patients were stratified using different

criteria; in the left panel (**a**) patients were stratified according to *BRCA*mut/del status with no significant difference in their PFS probability (p=0.14); in the middle panel (**b**) patients were stratified according to Telli et al, 2016 algorithm; in the right panel (**c**) patients were stratified using the ovaHRDscar algorithm and there is a significant difference (improvement) in PFS time (p = 0.024). **d** Hazard ratios (HR) for improvement of PFS in ovarian cancer patients using different criteria in two independent cohorts, the colors, rows and columns descriptions are the same as in Figure 2d. **e to f** Kaplan-Meier plots of PFS in the TERVA cohort, patients were stratified using different criteria; in the left panel (**e**) patients were stratified according to Telli et al, 2016 algorithm; in the right panel (**f**) samples were stratified using the ovaHRDscar. **g** Hazard ratios (HR) for improvement of PFS in the TERVA cohort, patients were stratified using different criteria the colors, rows and columns descriptions are the same as in Figure 2b. **h to j** Kaplan-Meier plots of OS in HERCULES patients and stratified using different criteria; in the left panel (**h**) patients were stratified according to *BRCA*mut/del status with no significant difference (p=0.045), in the middle panel (**i**) patients were stratified according to Telli et al, 2016 algorithm with no significant difference (p=0.022), in the right panel (**j**) samples were stratified using the ovaHRDscar algorithm and there is a significant difference (improvement) in PFS time (p = 0.006). **k** Hazard ratios (HR) for improvement of OS in ovarian cancer, patients were stratified using different criteria inside two independent cohorts, for every cox regression it was used as covariable the patient age at diagnosis, the rows, colors and columns descriptions are the same as in Figure 2h. **l to m** Kaplan-Meier plots of OS in the PCAWG cohort, at the left panel (**l**) the patients were stratified according to CHORD signature reported by developers, at the right panel (**m**) the patients were stratified according to ovaHRDscar approach. **n** Hazard ratios (HR) for improvement of OS in the PCAWG cohort, patients were stratified using different CHROD and ovaHRDscar criteria; the dot colors, rows and columns descriptions are the same as in Figure 2d.

Supplementary Figure 4. Differences in ovaHRDcar intra patient and relationship with tumor purity. **a** Difference in the ovaHRDscar values intra-patients and inter-patients in the

HERCULES prospective cohort (U test, p=1.95e-38)**. b** Schemed of the paired samples over treatment time, their purity and ovaHRDcar levels. **c** For each patient it was calculated the difference in ovaHRDscar and purity between every pair of their samples, no association between purity and ovaHRDscar difference (Pearson, p=0.4). **d** HR status classification using five different approaches to assess the ovaHRDscar values per patient (see results sections), per patient genomic alterations related with HR are shown. **e** Hazard ratios (HR) for improvement of PFS in the HERCULES cohort using different criteria to determine HR and under the five different approaches to assess the scar values (see results sections), for every cox regression it was used as covariable the residual tumor status (yes or no) after surgery, the colors, rows and columns descriptions are the same as in Figure 2b.

Figure 1

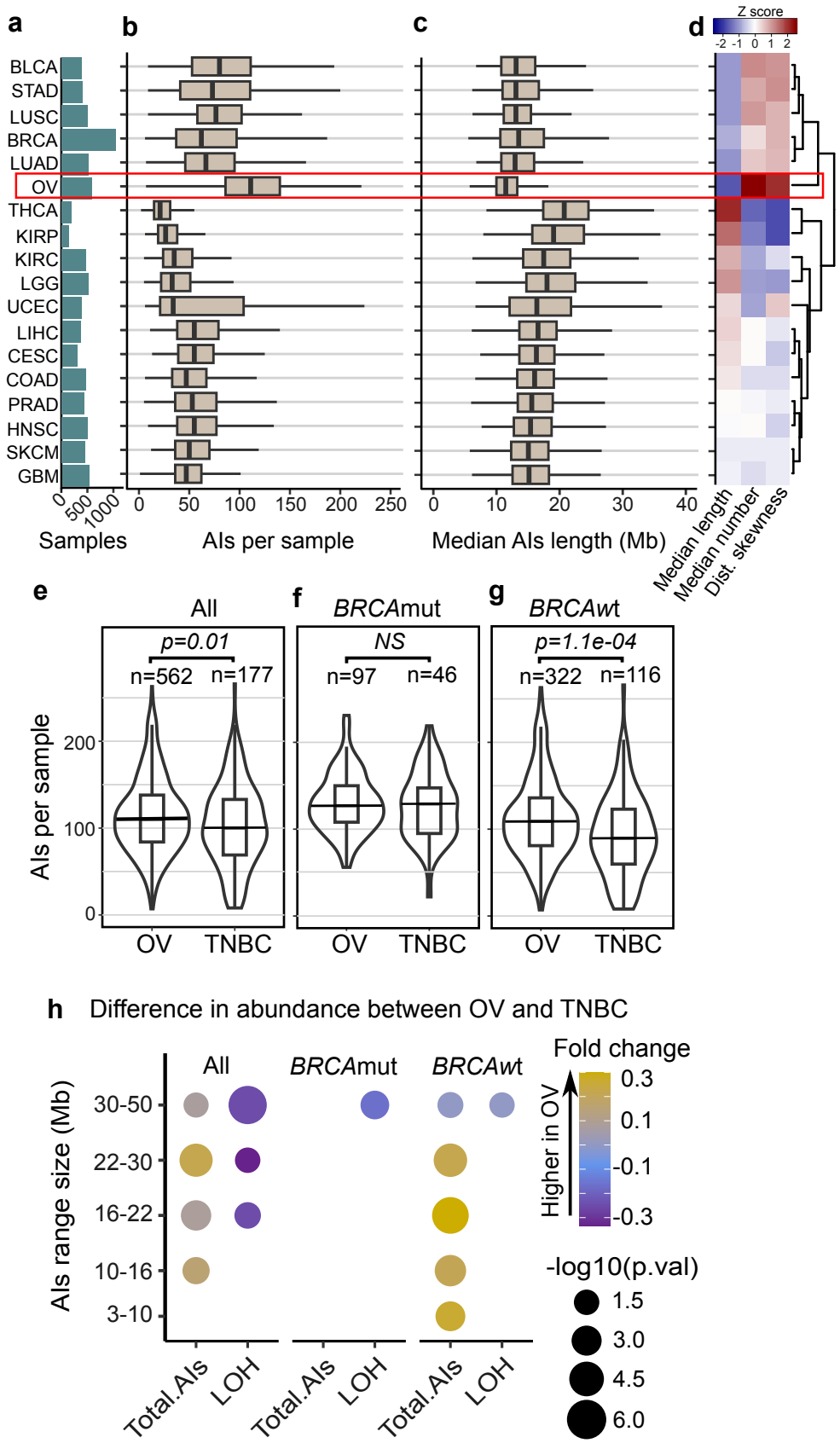
a
b
c
d
Z score
-2 -1 0 1 2
BLCA
STAD
LUSC
BRCA
LUAD
OV
THCA
KIRP
KIRC
LGG
UCEC
LIHC
CESC
COAD
PRAD
HNSC
SKCM
GBM
0 500 1000
Samples
0 50 100 150 200 250
AIs per sample
0 10 20 30 40
Median AIs length (Mb)
Median length
Median number
Dist. skewness
e
All
p=0.01
n=562 n=177
f
BRCAmut
NS
n=97 n=46
g
BRCAwt
p=1.1e-04
n=322 n=116
AIs per sample
0
100
200
OV TNBC
OV TNBC
OV TNBC
h Difference in abundance between OV and TNBC
All
BRCAmut
BRCAwt
AIs range size (Mb)
30-50
22-30
16-22
10-16
3-10
Total.AIs
LOH
Total.AIs
LOH
Total.AIs
LOH
Fold change
Higher in OV
0.3
0.1
-0.1
-0.3
-log10(p.val)
1.5
3.0
4.5
6.0

Figure 2

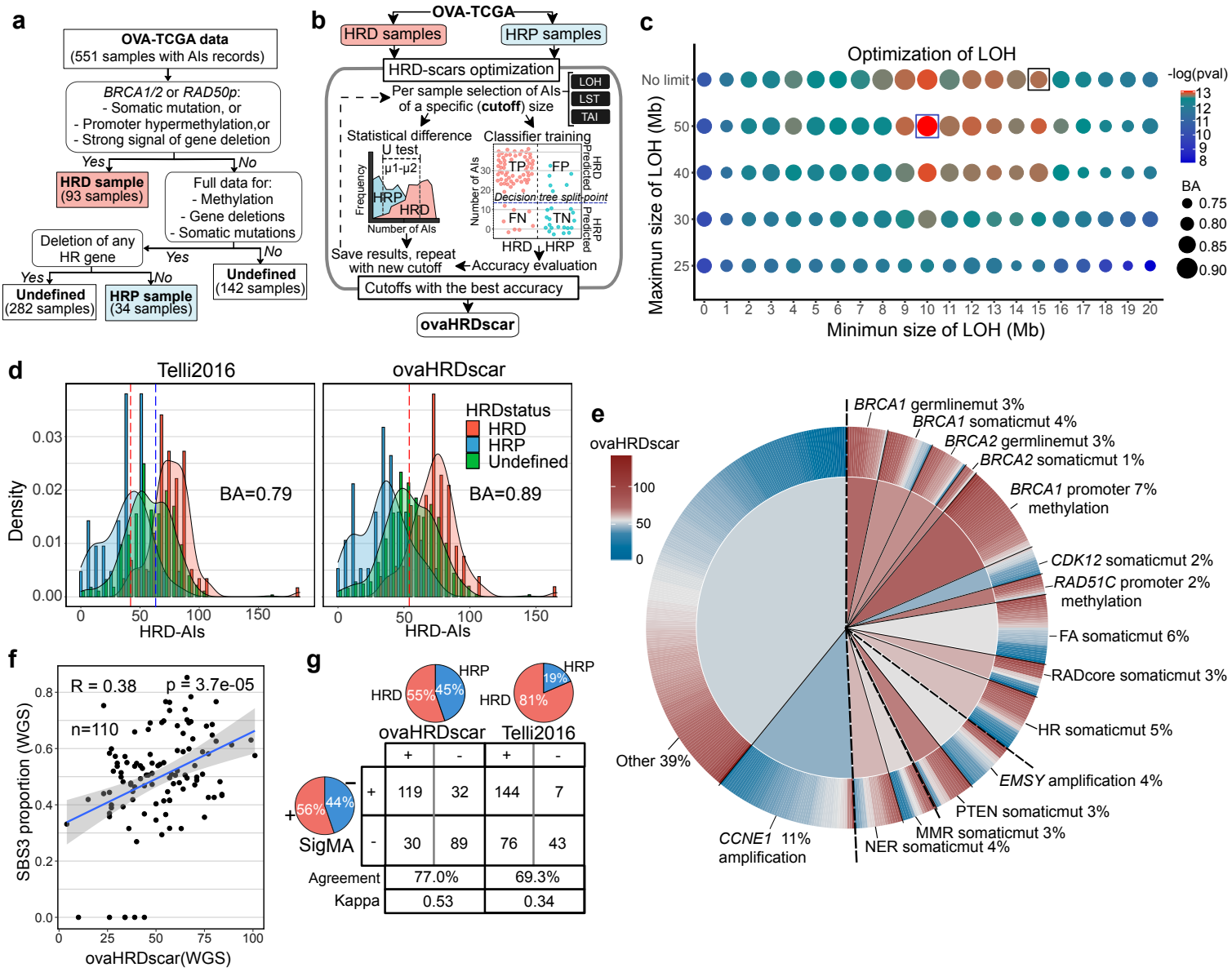

SigMA	ovaHRDscar +	ovaHRDscar -	Telli2016 +	Telli2016 -
+	119	32	144	7
-	30	89	76	43
Agreement	77.0%		69.3%	
Kappa	0.53		0.34	

Figure 3

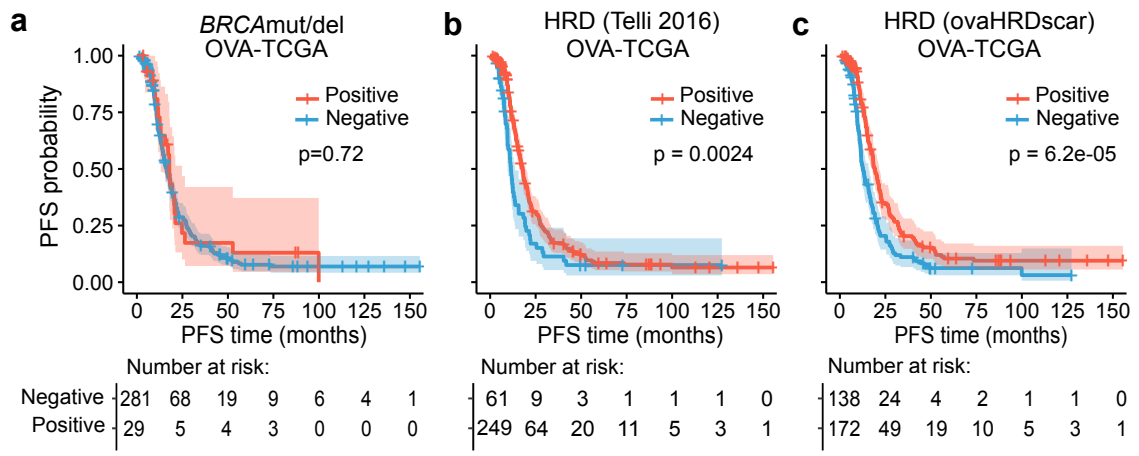

d *Cox model of PFS adjusted for residual tumor*

	OVA-TCGA n=310				OVA-TCGA* n=246				Hercules n=33			
All samples:	N	Prop	HR	Pval	N	Prop	HR	Pval	N	Prop	HR	Pval
*BRCA*mut/del	29	9%	0.855	0.0038	20	8%	0.671	0.015	5	15%	0.516	0.042
Telli2016	249	80%	0.467	1.6e−07	196	80%	0.479	1e−05	22	67%	0.682	0.037
Tacaya2020	146	47%	0.545	2.9e−07	108	44%	0.542	1.8e−05	14	42%	0.467	0.014
ovaHRDscar	172	55%	0.529	9.2e−08	131	53%	0.526	5.2e−06	16	48%	0.359	0.0061
*BRCA*mut/del excluded:	n=281				n=226				n=28			
Telli2016	220	78%	0.471	5.2e−07	176	78%	0.491	3e−05	17	61%	0.714	0.17
Tacaya2020	123	44%	0.537	1.1e−06	91	40%	0.533	3.9e−05	9	32%	0.509	0.093
ovaHRDscar	147	52%	0.523	3e−07	113	50%	0.521	1.1e−05	11	39%	0.379	0.046

Hazard-ratio (HR): 0.8 0.7 0.6 0.5 0.4

-log10(p.val): 3 4 5 6 7 | 2 3 4 5 | 0.9 1.2 1.5 1.8 2.1

*Excluding patients used for ovaHRDscar optimization

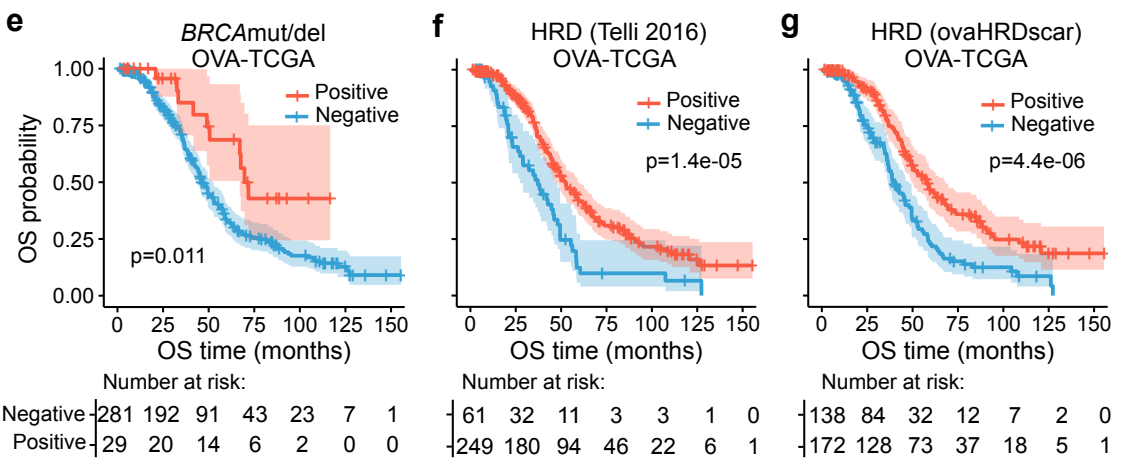

h *Cox model of OS adjusted for age at diagnosis*

	OVA-TCGA n=310				OVA-TCGA* n=246				PCAWG n=60			
All samples:	N	Prop	HR	Pval	N	Prop	HR	Pval	N	Prop	HR	Pval
*BRCA*mut/del	29	9%	0.485	0.0014	20	8%	0.453	0.016	13	22%	0.502	0.097
Telli2016	249	80%	0.481	1.9e−06	196	80%	0.44	6.2e−06	43	72%	0.506	0.067
Tacaya2020	146	47%	0.546	4.3e−06	108	44%	0.499	2.5e−05	20	33%	0.602	0.16
ovaHRDscar	172	55%	0.525	1e−06	131	53%	0.483	6.2e−06	28	47%	0.474	0.026
*BRCA*mut/del excluded:	n=281				n=261				n=47			
Telli2016	220	78%	0.51	1.3e−05	176	78%	0.459	2e−05	30	64%	0.593	0.22
Tacaya2020	123	44%	0.563	2.4e−05	91	40%	0.504	5.6e−05	11	23%	1.07	0.71
ovaHRDscar	147	52%	0.528	3.2e−06	113	50%	0.481	9.2e−06	17	36%	0.599	0.25

Hazard-ratio (HR): 1.0 0.6 0.5 0.4

-log10(p.val): 3 4 5 6 | 2 3 4 5 | 0.4 0.8 1.2

*Excluding patients used for ovaHRDscar optimization

Figure 4

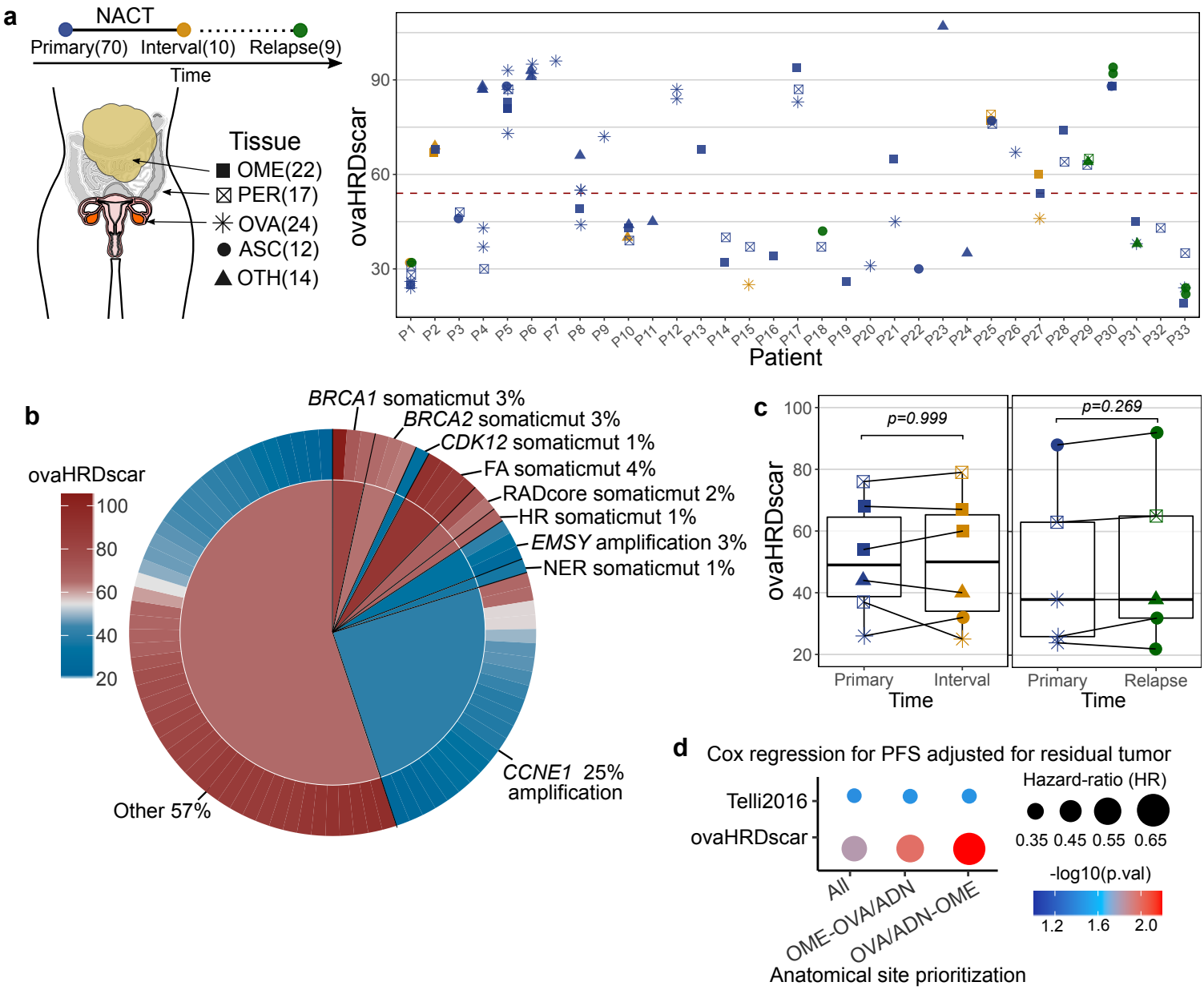
a
NACT
Primary(70)
Interval(10)
Relapse(9)
Time
Tissue
OME(22)
PER(17)
OVA(24)
ASC(12)
OTH(14)
ovaHRDscar
Patient
b
ovaHRDscar
BRCA1 somaticmut 3%
BRCA2 somaticmut 3%
CDK12 somaticmut 1%
FA somaticmut 4%
RADcore somaticmut 2%
HR somaticmut 1%
EMSY amplification 3%
NER somaticmut 1%
CCNE1 25% amplification
Other 57%
c
p=0.999
p=0.269
ovaHRDscar
Primary
Interval
Relapse
Time
d
Cox regression for PFS adjusted for residual tumor
Telli2016
ovaHRDscar
All
OME-OVA/ADN
OVA/ADN-OME
Anatomical site prioritization
Hazard-ratio (HR)
0.35 0.45 0.55 0.65
-log10(p.val)
1.2 1.6 2.0

Supplementary Figure 1

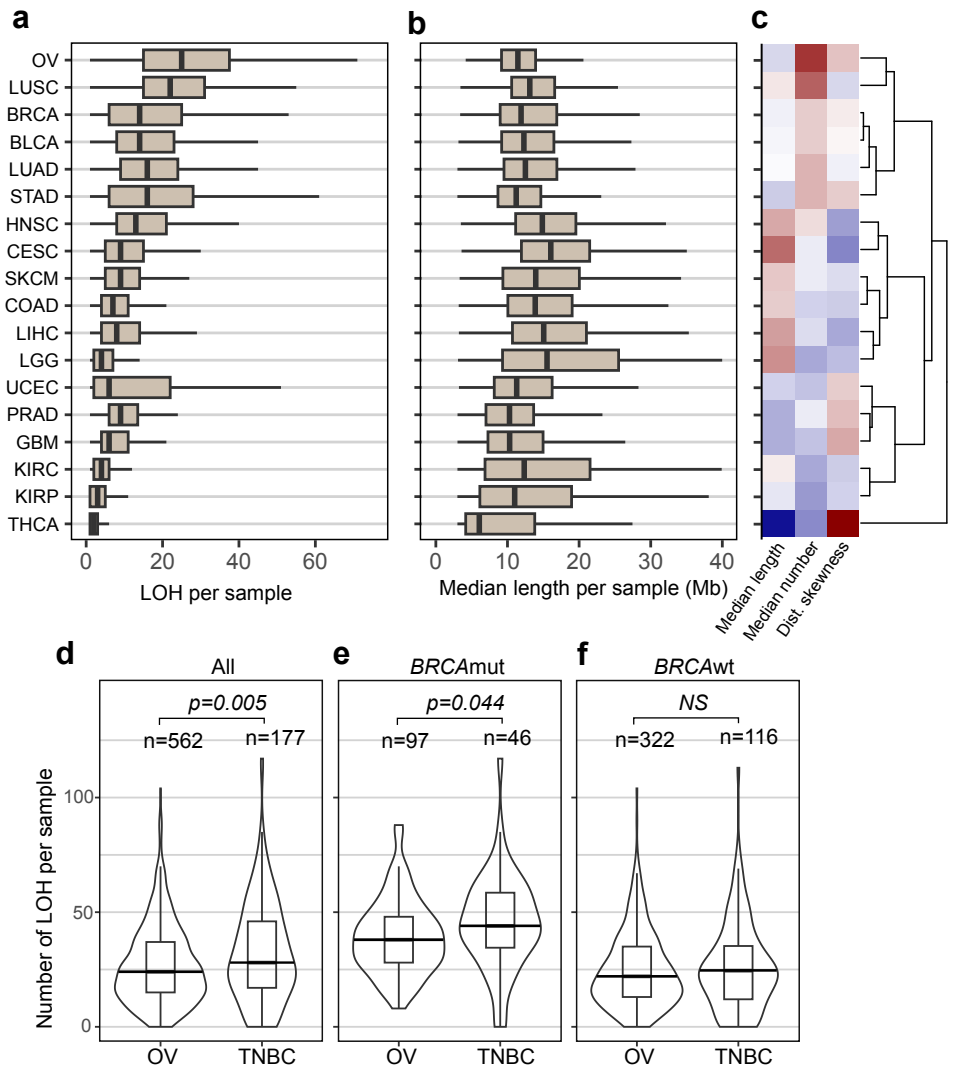

Supplementary Figure 2

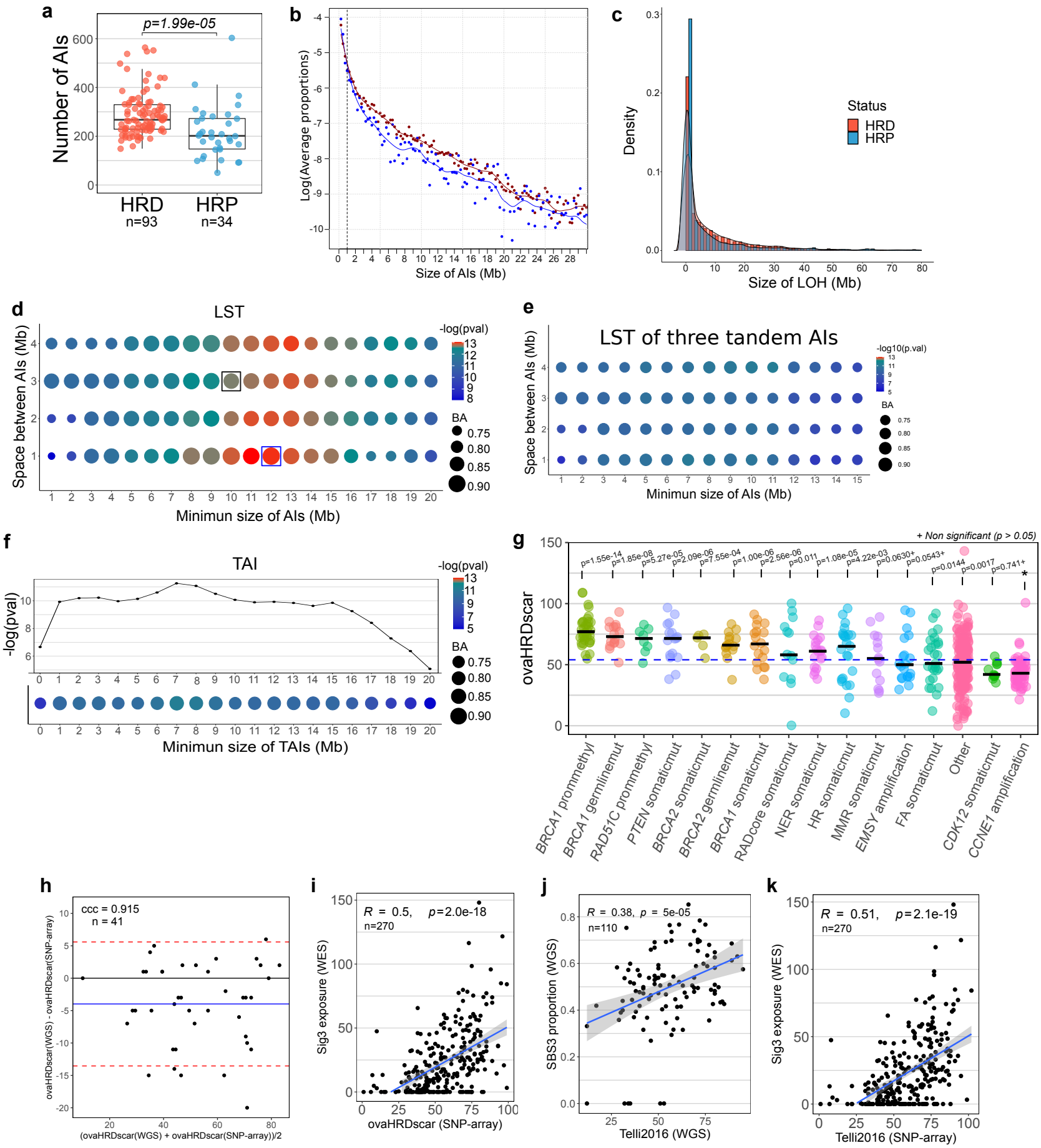

Supplementary Figure 3

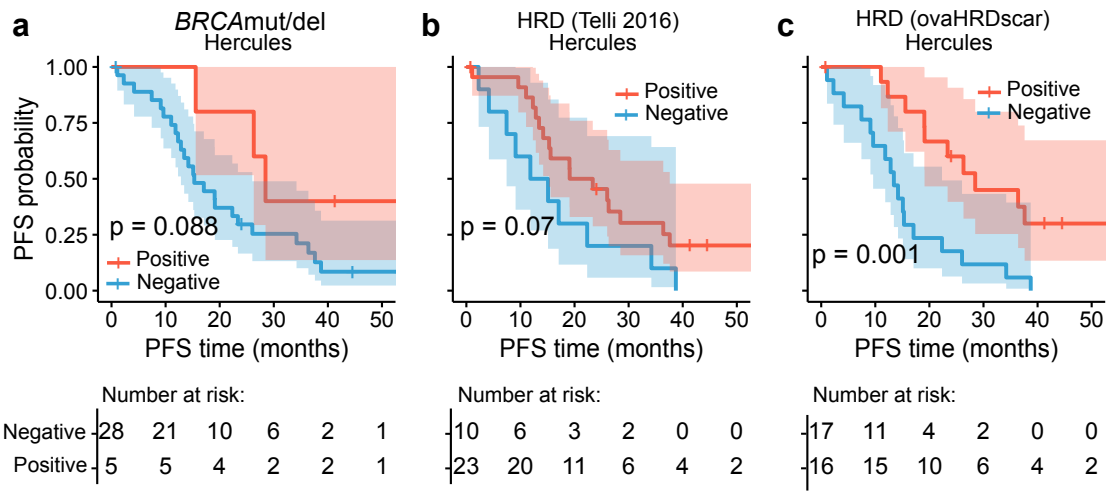

d *Cox model of PFS*

	OVA-TCGA n=310					Hercules n=33				
All samples:	N	Prop	HR	Pval		N	Prop	HR	Pval	
*BRCA*mut/del	29	9%	0.923	0.72	●	5	15%	0.364	0.1	●
Telli2016	249	80%	0.62	0.0026	●	22	67%	0.45	0.044	●
Tacaya2020	146	47%	0.59	4.8e−05	●	14	42%	0.36	0.015	●
ovaHRDscar	172	55%	0.601	7.4e−05	●	16	48%	0.279	0.0019	●
*BRCA*mut/del excluded:	n=281					n=28				
Telli2016	220	78%	0.62	0.0029	●	17	61%	0.541	0.14	●
Tacaya2020	123	44%	0.571	4.6e−05	●	9	32%	0.435	0.085	●
ovaHRDscar	147	52%	0.583	6.1e−05	●	11	39%	0.326	0.015	●

Hazard-ratio (HR): 0.8 0.7 0.6 0.5 0.4
-log10(p.val): 1 2 3 4
-log10(p.val): 1.0 1.5 2.0 2.5

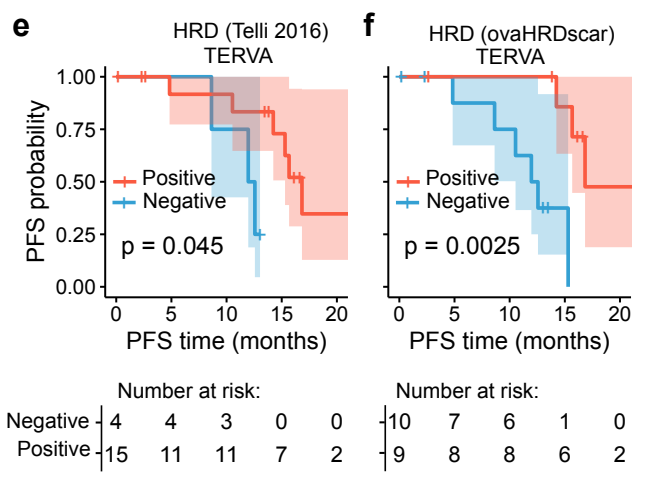

g *Cox model of PFS adjusted for residual tumor*

	TERVA n=20			
All samples:	N	Prop	HR	Pval
Telli2016	15	79%	0.191	0.190
Tacaya2020	7	37%	0.435	0.530
ovaHRDscar	9	47%	0.051	0.046

Hazard-ratio (HR): 0.4 0.3 0.2 0.1
-log10(p.val): 0.25 0.50 0.75 1.00 1.25

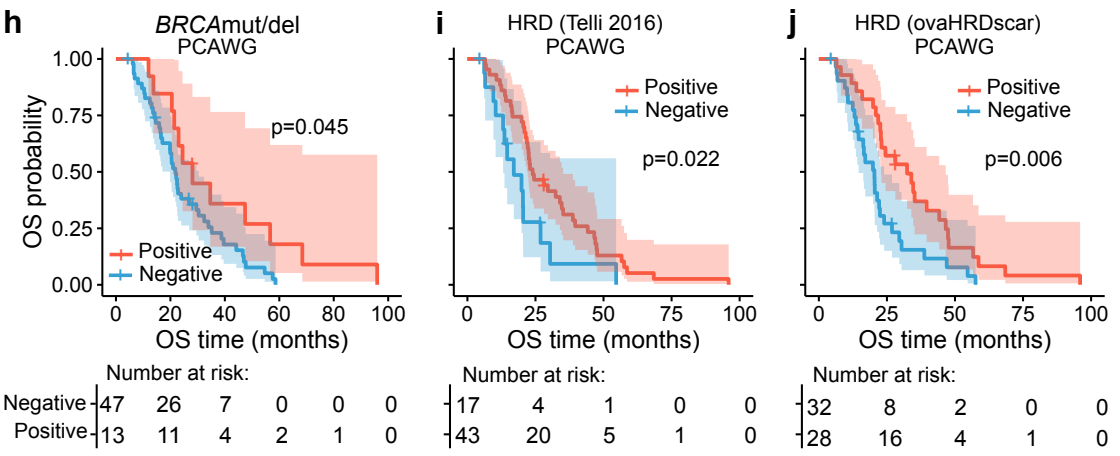

k *Cox model of OS*

	OVA-TCGA n=310					PCAWG n=60				
All samples:	N	Prop	HR	Pval		N	Prop	HR	Pval	
*BRCA*mut/del	29	9%	0.448	0.014	●	13	22%	0.495	0.049	●
Telli2016	249	80%	0.48	2.2e−05	●	43	72%	0.485	0.024	●
Tacaya2020	146	47%	0.522	1.3e−05	●	20	33%	0.58	0.071	●
ovaHRDscar	172	55%	0.515	6.4e−06	●	28	47%	0.465	0.0072	●
*BRCA*mut/del excluded:	n=281					n=47				
Telli2016	220	78%	0.515	0.00013	●	30	64%	0.571	0.097	●
Tacaya2020	123	44%	0.541	7.5e−05	●	11	23%	0.977	0.95	●
ovaHRDscar	147	52%	0.522	1.7e−05	●	17	36%	0.584	0.1	●

Hazard-ratio (HR): 1.0 0.6 0.5 0.4
-log10(p.val): 2 3 4 5
-log10(p.val): 0.5 1.0 1.5 2.0

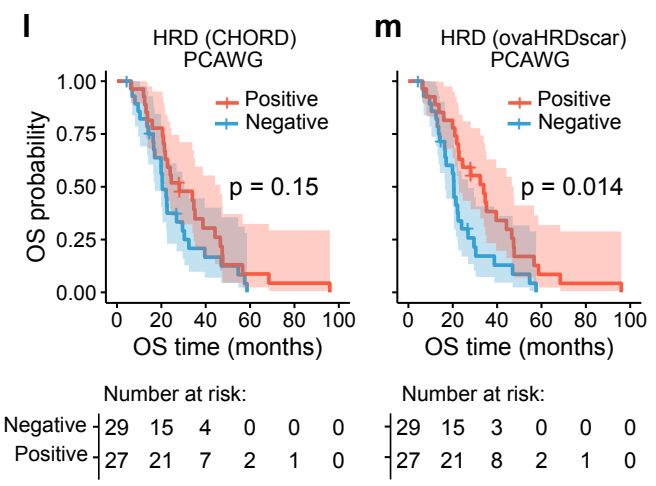

n *Cox model of OS*

	PCAWG n=56			
All samples:	N	Prop	HR	Pval
CHORD	27	48%	0.660	0.150
ovaHRDscar	27	48%	0.489	0.016

Hazard-ratio (HR): 0.65 0.60 0.55 0.50
-log10(p.val): 1.0 1.2 1.4 1.6
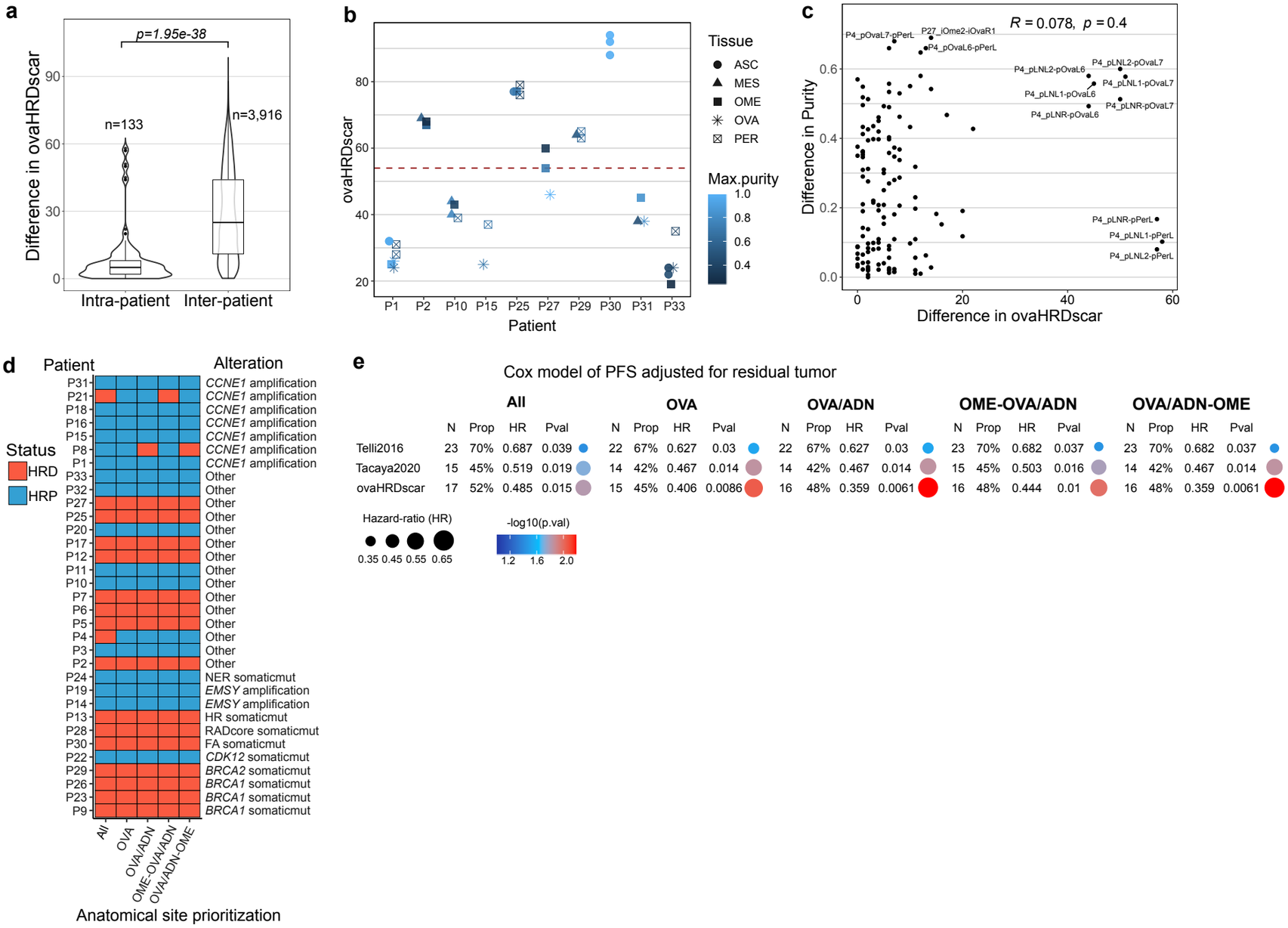
Supplementary Figure 4